

1 **Advection and non-climate impacts on the South Pole Ice Core**
2 Tyler J. Fudge¹, David A. Lilien^{1,2}, Michelle Koutnik¹, Howard Conway¹, C. Max Stevens¹,
3 Edwin D. Waddington¹, Eric J. Steig¹, Andrew J. Schauer¹, Nicholas Holschuh^{3,1}
4 ¹ Earth and Space Sciences; University of Washington, Seattle, WA 98195
5 ² Physics of Ice, Climate, and Earth; Niels Bohr Institute, Copenhagen, Denmark
6 ³ Department of Geology; Amherst College, Amherst, MA 01002
7 Email correspondence: tjfudge@uw.edu

8
9
10

11 **Abstract**

12 The South Pole Ice Core (SPICEcore), which spans the past 54,300 years, was drilled far from an
13 ice divide such that ice recovered at depth originated upstream of the core site. If the climate is
14 different upstream, the climate history recovered from the core will be a combination of the
15 upstream conditions advected to the core site and temporal changes. Here, we evaluate the
16 impact of ice advection on two fundamental records from SPICEcore: accumulation rate and
17 water isotopes. We determined past locations of ice deposition based on GPS measurements of
18 the modern velocity field spanning 100 km upstream, where ice of ~20 ka age would likely have
19 originated. Beyond 100 km, there are no velocity measurements, but ice likely originates from
20 Titan Dome, an additional 90 km distant. Shallow radar measurements extending 100 km
21 upstream from the core site reveal large (~20%) variations in accumulation but no significant
22 trend. Water isotope ratios, measured at 12.5 km intervals for the first 100 km of the flowline,
23 show a decrease with elevation of -0.008‰ m^{-1} for $\delta^{18}\text{O}$. Advection adds approximately 1‰ for
24 $\delta^{18}\text{O}$ to the LGM-to-modern change. We also use an existing ensemble of continental ice-sheet
25 model runs to assess the ice sheet elevation change through time. The magnitude of elevation
26 change is likely small and the sign uncertain. Assuming a lapse rate of 10°C per km of elevation,
27 the inference of LGM-to-modern temperature change is $\sim 1.4^{\circ}\text{C}$ smaller than if the flow from
28 upstream is not considered.

29
30
31
32

33 **1 Introduction**

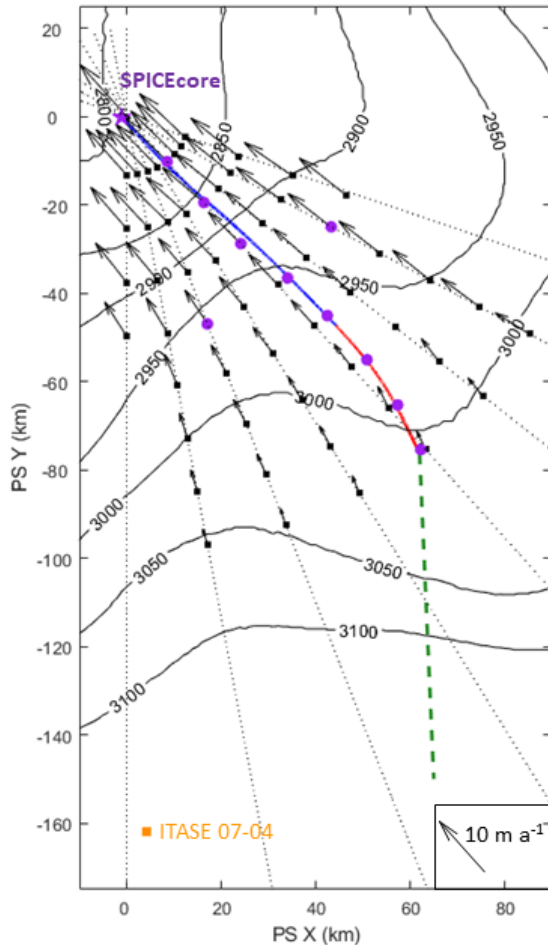
34 Ice cores provide unique and detailed records of past climate (e.g. Alley et al., 1993; Petit et al.,
35 1999; NorthGRIP, 2004; Marcott et al., 2014). Such records are most useful if they represent the
36 change in climate at a fixed geographic location and elevation. Two important non-climatic
37 influences on ice-core records are changes in ice-sheet elevation (Vinther et al., 2009; Steig et
38 al., 2001; Stenni et al., 2011; Parenin et al., 2007; Cuffey and Clow, 1997) and changes in the
39 location of ice origin due to flow (Whillans et al., 1984; Huybrechts et al., 2007; NEEM, 2013;
40 Steig et al., 2013; Koutnik et al., 2016). Many ice cores are drilled near an ice divide to minimize
41 both of these effects: ice thickness varies less in the interior than on the margins (Cuffey and
42 Paterson, 2010) and there is little lateral ice flow near a divide. The change in ice thickness can
43 be evaluated with ice-flow models (Parrenin et al., 2007; Golledge et al., 2014; Briggs et al.,
44 2014; Pollard et al, 2016) or measurements from the ice core itself (Martinerie et al, 1994; Steig
45 et al., 2001; Vinther et al., 2009; Waddington et al., 2005; Price et al., 2007). The magnitude and
46 sign of the elevation change in ice-sheet models varies depending on the specified boundary
47 conditions and model parameters, which have a large uncertainty (DeConto and Pollard, 2016;
48 Kingslake et al., 2018). We assess the ice-sheet elevation change near South Pole in this paper
49 using the 625-member ensemble of the Penn State ice-sheet model (Pollard et al., 2016). We also
50 focus on the impact of ice flow on the South Pole Ice Core (SPICEcore). We will use the term
51 “advection impact” to refer to variations in the ice-core histories that are due to variations in the
52 deposition location and paleo-elevation for different parcels of ice in the South Pole core, as
53 opposed to temporal change in the climate at the ice-core site.

54
55 Ice cores are often drilled far enough from divides that lateral advection is important because of
56 site characteristics (NorthGRIP, 2004; EDML, EPICA 2006; WAIS Divide, Morse et al., 2005;
57 NEEM, 2013), logistical considerations (Camp Century, Gow et al., 1968; Dye-3, Dansgaard et
58 al., 1969; Byrd, Hammer et al., 1980; Vostok, Lorius et al., 1985), or concern about divide
59 migration over the drill site (Waddington et al., 2001). The importance of advection on ice-core
60 records depends on both the velocity of the ice and the gradient in the constituent or property of
61 interest. For well-mixed atmospheric gases, such as carbon dioxide and methane, there is no
62 direct impact on the histories. The affected histories are primarily those recovered from the ice
63 phase: accumulation rate, water isotopes, surface temperature, and aerosols. Of the cores that
64 have been drilled off of ice divides, the horizontal velocities range from less than 1 m a^{-1}
65 (EDML) to 12 m a^{-1} (Dye 3) and all require correction to obtain the climate history for a fixed
66 geographic location (Whillans et al., 1984; Steig et al., 2001; Huybrechts et al., 2007; Vinther et
67 al., 2009; NEEM, 2013; Steig et al., 2013; Koutnik et al., 2016).

68
69 The 1750 m long SPICEcore was obtained at the South Pole between 2014 and 2016.
70 SPICEcore was sited, in part, to take logistical advantage of South Pole station where the surface
71 velocity is 10 m a^{-1} in the direction of 40°W (Hamilton, 2004; Casey et al., 2014). Lilien et al.
72 (2018) inferred the flowline out to 100 km upstream and concluded that Titan Dome is the likely
73 source region for ice reaching the SPICEcore site. Previous measurements of water isotope
74 values upstream of South Pole are primarily from surface snow samples, which do not provide
75 reliable time-averaged values (Masson-Delmotte et al., 2008; Dixon et al., 2013). A shallow ice
76 core near Titan Dome (US-ITASE 07-4) provides a single estimate of accumulation (0.074 m ice
77 equivalent a^{-1} ; Dan Dixon, personal communication). Here, we assess the advection impact (i.e.,

78 non-climate impact) on the accumulation-rate, water-isotope, and surface-temperature histories
79 of SPICEcore using new measurements in the upstream catchment.

80



82

83 Figure 1: Map of the area upstream of
84 the South Pole. SPICEcore location is
85 purple star. 10 m core locations are
86 purple circles. Stake locations (black
87 squares) were surveyed with GPS in
88 multiple years to measure velocity
89 vectors. Flowline was inferred from the
90 velocity measurements for past 10.1 ka
91 (blue, from Lilien et al., 2018) and 10.1
92 ka to ~25 ka (red). Unconstrained
93 flowline for ~25 ka to 55 ka is dashed
94 green. Surface topography contours are
95 from BedMap2 (Fretwell et al., 2013).
96 ITASE 07-04 core at Titan Dome is
97 orange square. Note that Titan Dome is
98 a broad ridge and the geometry is not
99 well defined in BedMap2; the elevation
100 does not match the 3090 m measured by
101 Dixon et al. (2013).

81

102 2 Methods

103 To assess the impact of advection on the SPICEcore climate histories, we measured ice velocity,
104 accumulation rates, water isotopes, and firn temperatures in the upstream catchment. The surface
105 ice-flow velocities, inferred flowline, and spatial pattern of accumulation were described by
106 Lilien et al. (2018; <http://www.usap-dc.org/view/dataset/601100>) and we provide only a brief
107 review below.

108

109 2.1 Surface Ice-flow Velocity and Flowline Determination

110 Determining the ice-flow velocity near South Pole is more difficult than many other
111 locations in Antarctica; there is little satellite coverage due to the geometry of satellite orbits
112 resulting in a data “pole hole.” Rignot et al. (2011) used synthetic aperture radar to compute the
113 surface velocity, but utilized a substantially tilted satellite view, resulting in velocity
114 measurements that are not sufficiently precise to define the flowline. To obtain improved
115 velocity measurements in the region, we performed repeat surveys of stakes with GPS during

116 four consecutive field seasons. We installed 56 stakes at 12.5 km intervals along lines of
117 longitude from 110°E to 180°E at 10° intervals (Lilien et al., 2018). The 110° and 180° lines
118 were measured only to 50 km from South Pole; the others were measured to 100 km (Figure 1).
119 The measured velocities range from 3 to 10 m a⁻¹, with errors of ±0.02 to 0.25 m a⁻¹ in each
120 horizontal direction.

121

122 **2.2 Accumulation Rate**

123 The accumulation rate along the flowline is derived from radar layers imaged from
124 approximately 20 m to 100 m depth with a 200 MHz radar (details can be found in Lilien et al.,
125 2018). The depth of a radar layer is converted to an accumulation rate using the density profile
126 and depth-age relationship of a core extracted by us on the flowline 50 km upstream from
127 SPICEcore. The firn depth-density profile is assumed to be unchanging along the flowline. The
128 firn density affects the derived accumulation rate history both through the inferred depth of the
129 layer due to the radar-wave propagation speed and through the conversion to ice-equivalent
130 thickness. These two uncertainties oppose each other but do not necessarily cancel. Using four
131 additional density profiles near South Pole, Lilien et al. (2018; Figure S4) found the spread in
132 accumulation has a standard deviation of 2.3% for a layer at ~20 m depth. Deeper layers have a
133 smaller spread because the density is most variable near the surface. All accumulation rates are
134 given in m a⁻¹ of ice equivalent.

135

136 **2.3 Water Isotopes**

137 Water isotopes ratios of δ¹⁸O and δD were measured in cores of approximately 10 m depth at
138 12.5 km spacing along the flowline, as well as at two sites 15 km perpendicular to the flowline
139 50 km upstream of SPICEcore, for a total of 10 firn cores. We also report the deuterium excess,
140 using the log definition (d_{ln}; Markle et al., 2017). The cores were sampled at 0.5 m intervals in
141 the field and allowed to melt in plastic bottles. The measurements were performed at the
142 University of Washington's Isolab with a Picarro L-2120i. The average δ¹⁸O and δD values (vs
143 Vienna Standard Mean Ocean Water) for each core are presented here. The cores were not dated
144 and thus the water isotopes cannot be averaged over the same ages; averaging using only the
145 upper 5 m for each core instead of the full core produced negligible differences. One outlier from
146 0.5-1 m depth at site 25 km was excluded.

147

148 **2.4 10 m Temperatures**

149 The temperature at approximately 10 m depth was measured in each borehole left by the
150 shallow-core extraction. We averaged the values measured by four thermistors surrounded by a
151 copper shield. The thermistors were left in the borehole for different lengths of time ranging
152 from 28 minutes to 48 hours.

153

154 **2.5 Analysis of Continent-scale Ice Sheet Models**

155 We use a 625-member ensemble of the Penn State ice-flow model (Pollard et al., 2016) to assess
156 possible ice-sheet changes during the deglacial transition. The model uses a 20-km grid size for
157 West Antarctica, which includes the South Pole region. The accumulation rate applied at 20 ka is
158 approximately half of the modern value (Pollard and DeConto, 2012). The ensemble is used to
159 assess the histories of surface velocity and elevation of the South Pole. The ensemble varies four
160 different ice-dynamic parameters with five values each. The four parameters affect the basal
161 sliding coefficient where ice is no longer grounded (CSHELF); ice shelf melt rate (OCFAC);

162 calving rate factor (CALV); and isostatic rebound (TAUAST). We perform evaluations using
 163 both the full ensemble (n=625) and a subset, including only the parameter values identified with
 164 the advanced statistical techniques (n=32) to best fit geologic constraints (Table 1; Pollard et al.,
 165 2016, Figure 3, right column).

166 Table 1: Pollard et al. (2016) most likely parameter values

Parameter	Abbreviation	Value	Unit
Basal sliding coefficient in modern oceanic areas	CSHELF	-6 and -5	$10^x, m a^{-1} Pa^{-2}$
Bedrock-elevation isostatic relaxation time	TAUAST	1, 2, 3 and 5	kyr
Calving rate factor	CALV	1 and 1.3	non-dimensional
Melt-rate coefficient at base of ice shelves	OCFAC	1 and 3	non-dimensional

167
 168

169 3 Results

170 3.1 Gradients in Upstream Climate

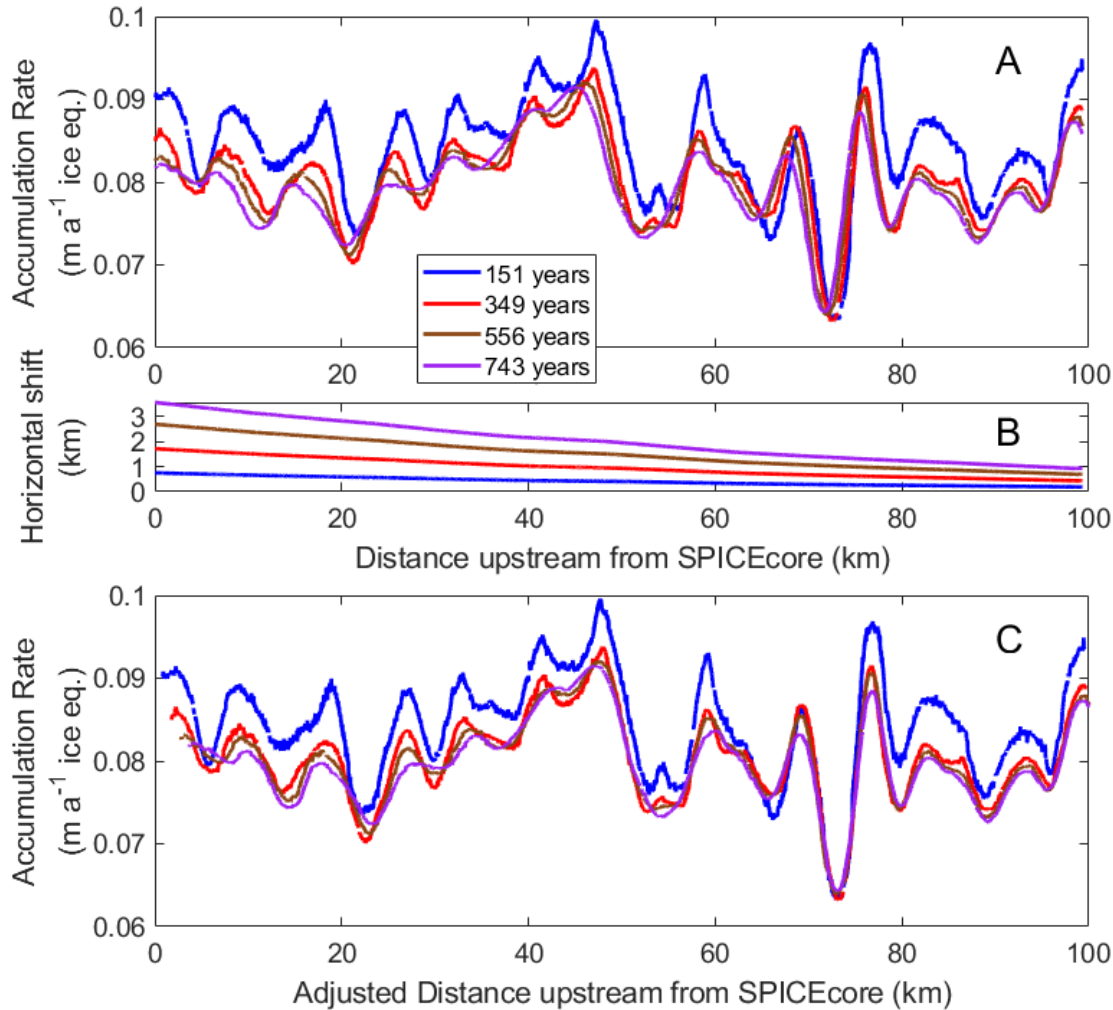
171 3.1.1 Accumulation Rate

172 The accumulation rate along the 100 km flowline for four different internal layers is shown in
 173 Figure 2. The youngest layer is 151 years before 2017 (~20 m depth) and was used by Lilien et
 174 al. (2018); the 743-year layer is the deepest (~90 m) layer resolved. Although the layers are
 175 relatively young, there can still be a horizontal offset of hundreds of meters to kilometers from
 176 where the layer was deposited on the surface. In Figure 2A, the accumulation rates in the upper
 177 panel are plotted at the position of the radar trace. The impact of horizontal advection can be
 178 observed as the older layers appear shifted to the left (closer to SPICEcore) compared to the
 179 younger layers.

180
 181 To account for horizontal advection, the position where the accumulation rate is inferred (i.e. the
 182 location of the radar trace) is adjusted. This adjustment is made by multiplying the half-age of
 183 the layer by the surface velocity at the mid-point of its path from deposition to the current trace
 184 location (Figure 2B). The adjustment ranges from 3.7 km at SPICEcore for the 743-year layer to
 185 0.2 km for the 151-year layer at the upstream end. Shifting the distance of the accumulation
 186 records (Figure 2C) better aligns the peaks and troughs among the four layers. It also highlights
 187 that older layers vary less along flow. The depth of a layer reflects the average surface
 188 accumulation rate over the distance traveled. Thus, an older layer is flatter because it averages
 189 the influence of accumulation on vertical velocity over a longer distance (Waddington et al.,
 190 2007). This shows that simply shifting the position of the layers to account for horizontal
 191 advection does not fully recover the spatial variations in accumulation.

192
 193 A more-complete treatment could solve an inverse problem to infer the surface accumulation rate
 194 along the flow line that best matches the observed layer thicknesses (e.g., Waddington et al.,
 195 2007). We do not address this because here we focus on the advection impact on the SPICEcore
 196 record and not a formal evaluation of the surface accumulation patterns consistent with available
 197 layers. Lilien et al. (2018, supplement) showed that the 151-year layer was sufficiently deep to
 198 record real climate variations, and not noise, but shallow enough to not be significantly affected
 199 by lateral flow.

200

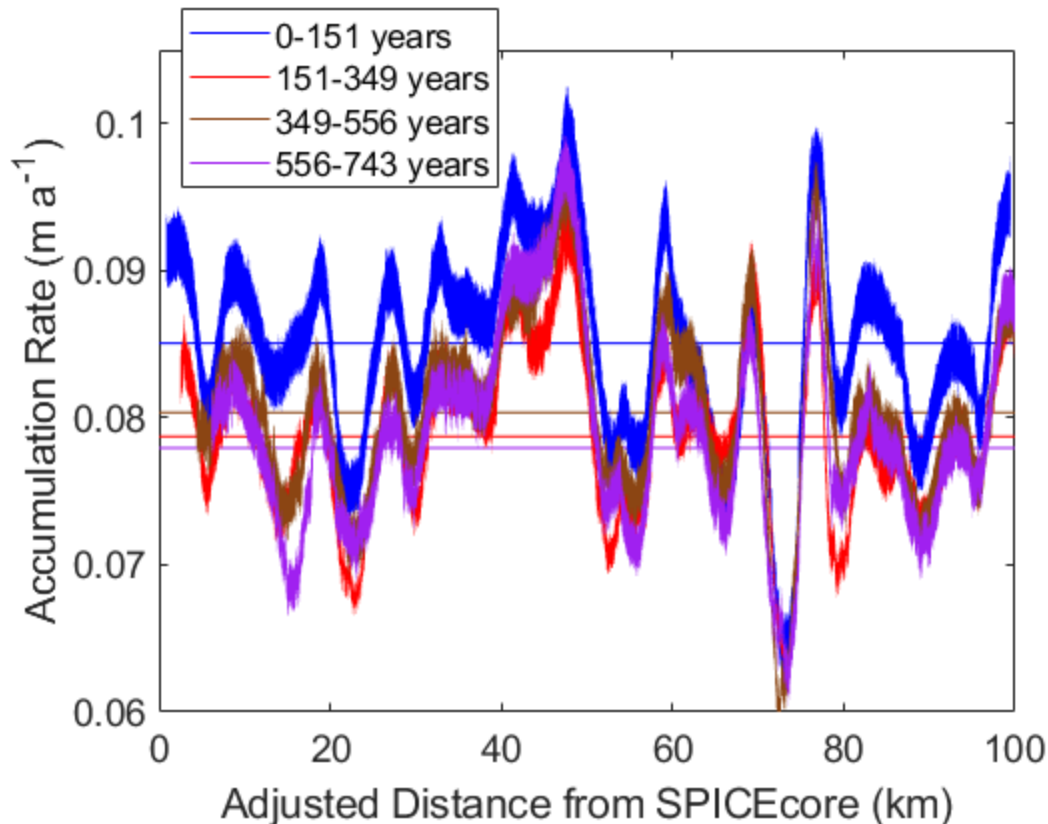


202
 203 Figure 2: Accumulation rate along flowline. Panel A shows the accumulation rate for four radar
 204 layers, with ages in years before 2017. Panel B shows average horizontal distance traveled. Panel
 205 C shows same inferred accumulation as in Panel A, with the position adjusted to account for the
 206 horizontal distance traveled.

207
 208 The average accumulation rate of the oldest (743-year-old) layer is 0.080 m a^{-1} and the spatial
 209 linear trend of $-4 \times 10^{-6} \text{ m a}^{-1} \text{ km}^{-1}$ is negligible. Shorter-wavelength spatial variations are
 210 approximately $\pm 20\%$ of the average value, much larger than the linear trend. Beyond the 100 km
 211 of mapped flowline, the only accumulation-rate information is from the US-ITASE 07-04 core
 212 near Titan Dome, where an accumulation rate of 0.074 m a^{-1} was inferred (Daniel Dixon,
 213 personal communication, 2013). This is within the range of accumulation rates identified along
 214 the flowline, but slightly smaller than the 0.080 m a^{-1} average along the first 100 km of the
 215 flowline. With only a single point measurement, we cannot resolve whether this accumulation
 216 rate near Titan Dome is representative of a mean value for a wider area.

217

218 We also calculate the accumulation rate for the intervals between successive layers (Figure 3),
 219 which allows temporal trends to be more clearly evaluated. The uncertainty in the accumulation
 220 rate is greatest for the 151-year layer because the density measurements are least certain in the
 221 lower-density surface snow, and surface firn conditions are more spatially variable. We calculate
 222 the uncertainty for an interval based on the density profiles of five different firn cores (the core
 223 we drilled at 50 km and four cores from near South Pole; Severinghaus et al., 2001; Christo
 224 Buizert, personal communication). The uncertainty shading shown in Figure 3 is the range
 225 between the maximum and minimum accumulation rates using the five density profiles. The
 226 spatial average of the three older intervals are within uncertainty of each other. The spatial
 227 average of the 0 to 151-year interval is always greater than the older three intervals. Because the
 228 spatial average of the minimum accumulation rate (based on firn density) for 0 to 151-year is
 229 greater than the spatial average of the maximum for the older intervals, we have confidence that
 230 the accumulation rate has increased in the past 151 years. The accumulation increase is $8 \pm 4\%$
 231 compared to the previous 592 years (151 to 743 years before 2017). Previous ice-core estimates
 232 of accumulation at South Pole suggested an increase in the past 150 years (e.g. Ferris et al.,
 233 2011), but an increase could not be identified with confidence because variations among cores
 234 were dominated by spatial, not temporal, effects (van der Veen et al., 1999). Our measurements
 235 average over a 100 km distance allowing the temporal change to be identified.
 236



237
 238 Figure 3: Temporal average accumulation rate for ages between radar layers. Shading indicates
 239 uncertainty based on five firn-density profiles. Distance from SPICEcore has been adjusted as in
 240 Figure 2 and described in main text. Horizontal lines indicate spatial average of the accumulation
 241 rate using the density profile measured on the firn core at 50 km.
 242

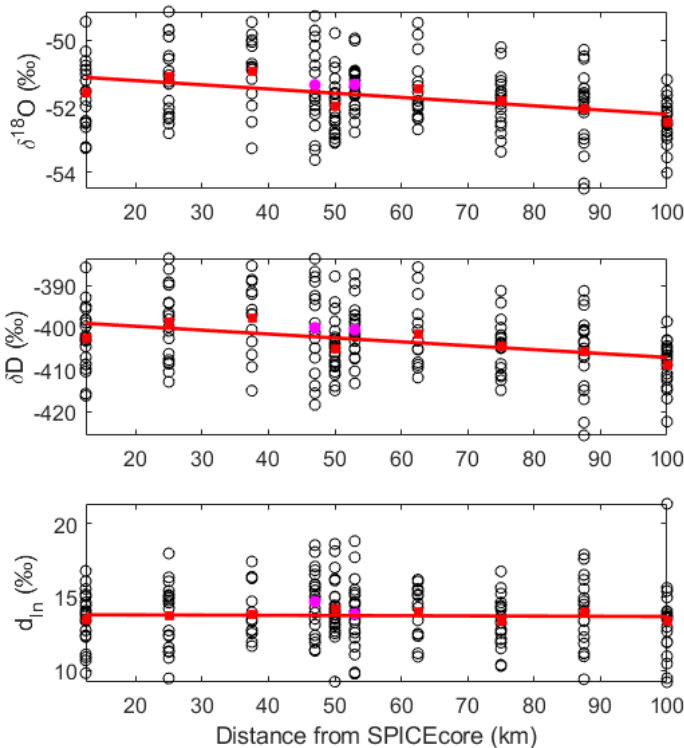
Interval	Mean	Minimum	Maximum
151-349	8%	4%	12%
349-556	6%	1%	11%
556-743	9%	3%	13%
151-743	8%	4%	12%

Mean increase uses density profile from the core at 50km for all layers

Minimum (maximum) increase uses density profile which yields the minimum (maximum) accumulation rate for the 0-151 interval and the density profile which yields the maximum (minimum) for the older layers.

243 3.1.2 Water Isotopes

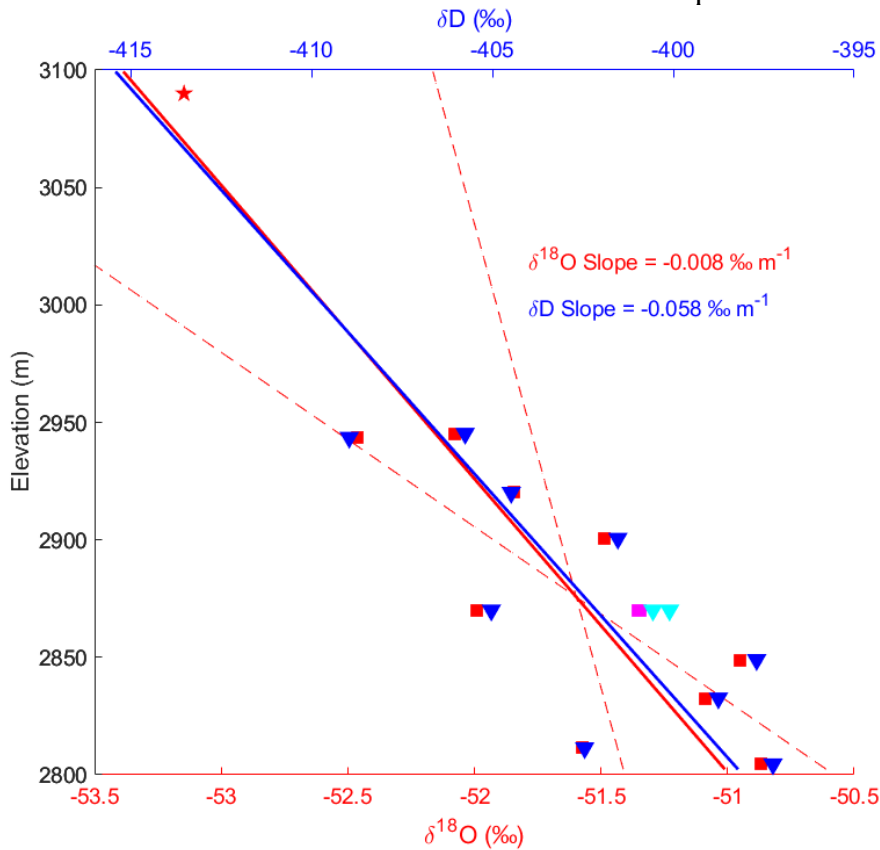
244 Measurements of water isotopes require the collection of ice samples and thus have less spatial
 245 resolution than the radar-derived accumulation-rate measurements. There is considerable scatter
 246 (Figure 4) in the 0.5 m resolution samples, which have durations of a few years (i.e. 2-4 years)
 247 per sample; the differences among 0.5 m samples are likely driven by interannual variations.
 248 Using the mean values, a decrease with distance from South Pole is observed in both $\delta^{18}\text{O}$ and
 249 δD . The d_{In} values show no significant trend upstream.
 250



251 Figure 4: Water-isotope values (black circles) and averages (red squares) for shallow cores along
 252 the flowline upstream of South Pole. Cores at 50 km upstream on 120°E and 160°E are plotted at
 253 47 km and 53 km (magenta circles). Linear slope (thick red line) is from the average values
 254 along the flowline only.
 255

256
257
258
259
260
261
262
263
264
265
266

The $\delta^{18}\text{O}$ and δD values plotted by elevation are shown in Figure 5. Linear fits to $\delta^{18}\text{O}$ and δD yield slopes of $-0.0080 \pm 0.0055 \text{‰ m}^{-1}$ and $-0.0579 \pm 0.04 \text{‰ m}^{-1}$ respectively (95% confidence levels). Our value for $\delta^{18}\text{O}$ is in between the slope of -0.009‰ m^{-1} from the Masson-Delmotte et al. (2008) database and the slope of -0.007‰ m^{-1} found in their multiple linear regression analysis which includes latitude and distance from the coast. Including the average $\delta^{18}\text{O}$ value from the upper 1.2 m of the US-ITASE 07-04 firn core at Titan Dome (-53.15‰) in the linear regression changes the slope to -0.0073‰ m^{-1} , which is in good agreement with the mean slope. Because the Titan Dome value is an average of the upper 1.2 m and not directly comparable in time to our 10 m average measurements, we use the mean slope of 0.008‰/m^{-1} from the 10 m cores for the advection correction described in the subsequent section.



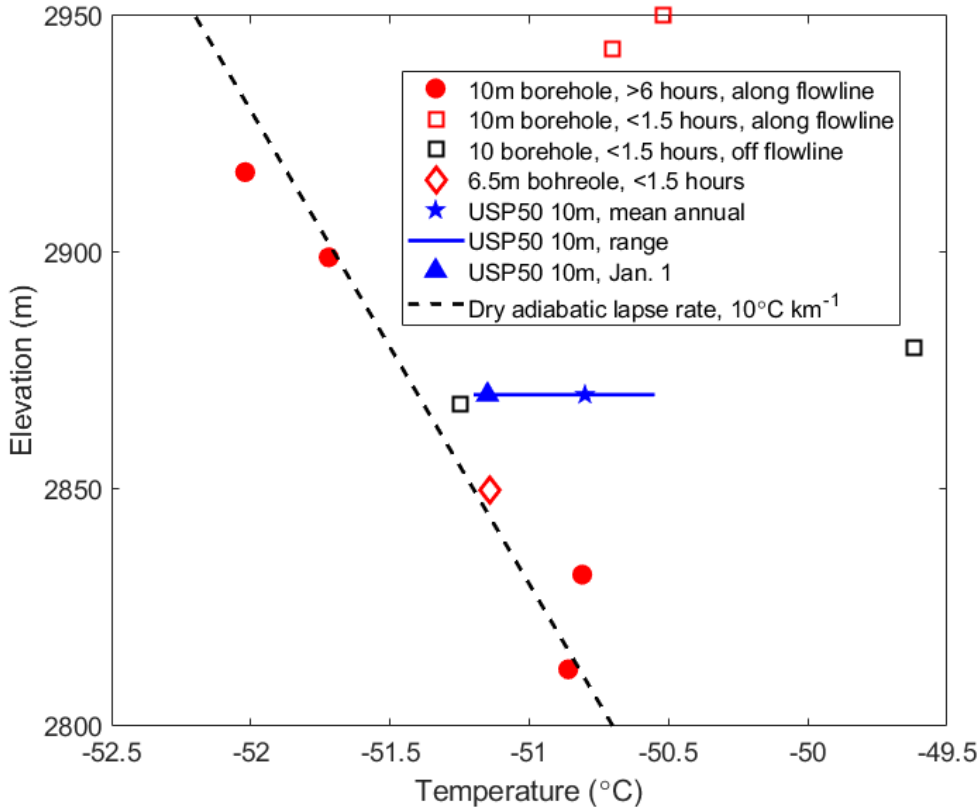
267
268
269
270
271
272
273
274
275

Figure 5: Average $\delta^{18}\text{O}$ (red squares) and δD (blue triangles) values from the 10 m cores along the flow line and SPICEcore. Average $\delta^{18}\text{O}$ and δD from cores off of the flowline at 50 km upstream (pink squares and cyan triangles). $\delta^{18}\text{O}$ of US-ITASE 07-04 core at Titan Dome (red star). Linear fit of 10 m cores along the flow line for $\delta^{18}\text{O}$ (red thick line) and δD (blue thick line) do not include Titan Dome or cores from off the flowline. 95% confidence intervals of the $\delta^{18}\text{O}$ fit (red dashed lines) are shown. Confidence intervals of δD overplot those of $\delta^{18}\text{O}$ and are not shown.

276 3.1.3 Surface Temperature Gradient

277 The ~ 10 m temperatures are shown in Figure 6. Unfortunately, time constraints in the field
278 forced differences in the measurement procedure between sites, preventing a determination of
279 the gradient in mean annual temperature. Measurements that equilibrated for less than 1.5 hours

280 yielded warmer temperatures than those left in boreholes for longer times, and we consider those
 281 shorter measurements less reliable. Measurements that were made after leaving the thermistors in
 282 the boreholes for longer than six hours are consistent with a dry adiabatic lapse rate of $10^{\circ}\text{C km}^{-1}$
 283 ¹, but we cannot reject a wide range of other values for the lapse rate.



284 Figure 6: Temperature measurements. Filled symbols equilibrated for more than 6 hours; open
 285 symbols equilibrated for less than 1.5 hours. Red symbols are along the flow line; black symbols
 286 are off the flowline. Diamond is a measurement at 6.5 m depth, which is likely $\sim 0.7^{\circ}\text{C}$ colder
 287 due to the winter cold wave than if measured at 10 m depth. Blue symbols are from a single
 288 thermistor installed at 10 m depth in a back-filled borehole with measurements recorded for more
 289 than 1 year; star is mean annual temperature, triangle is initial temperature after equilibration and
 290 horizontal line is the range of temperature recorded. Black dashed line shows a lapse rate of
 291 $10^{\circ}\text{C km}^{-1}$.
 292
 293

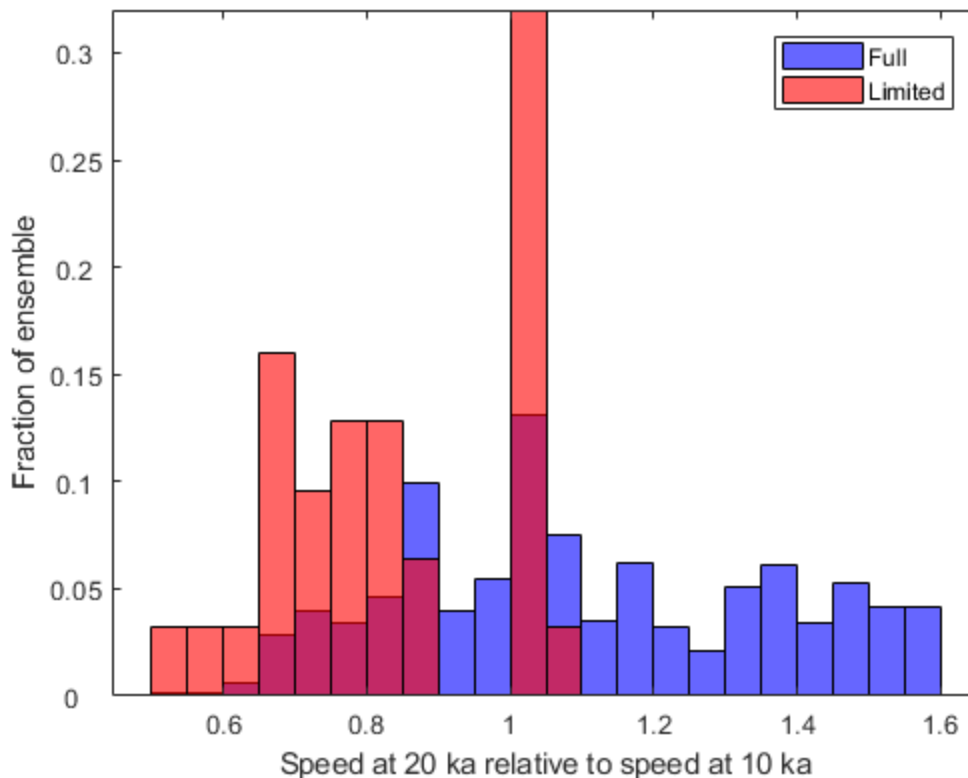
294 3.2 Determination of Flowline Position and Age

295 We divide the reconstruction of the flowline into three segments based on the data available for
 296 different distances upstream from SPICEcore:

- 297 1) 0 to 65 km (0 to 10.1 ka) which has been constrained by Lilien et al. (2018)
- 298 2) 65 to 100 km (10.1 to ~ 25 ka) where we have velocity measurements
- 299 3) beyond 100 km (older than ~ 25 ka) where only limited data from other sources exist

300 The uncertainty associated with the reconstruction increases for each segment because of the
 301 data available as well as possible changes to the ice-sheet configuration at earlier times. For
 302 segment 1, the uncertainty is low because correlation of the SPICEcore layer thicknesses and
 303 upstream accumulation pattern provides a unique and tight constraint (Lilien et al., 2018). For

304 segments 2 and 3, we have no inferences of past ice-sheet velocity. The variation in horizontal
 305 velocity with depth does not need to be considered because we are only interested in tracking
 306 particles to 1750 m depth in SPICEcore where the modeled horizontal velocity is at least 99% of
 307 the surface velocity. The challenge of determining the flowline position with age is then of
 308 estimating the past surface velocity. The modeled surface velocities near South Pole in the ice-
 309 sheet ensemble (Pollard et al., 2016) are slower than observed (mean of 2 m a^{-1} for the models
 310 runs compared to the measured 8 m a^{-1} at $\sim 20 \text{ km}$ from SPICEcore) and thus cannot be used
 311 directly. Instead, we use the relative change in speed between 20 ka and 10 ka to inform our
 312 choice of speed change for this time period. The full ensemble (Figure 7) shows a large fraction
 313 of model runs with faster velocities at 20 ka compared to 10 ka with a mean slowdown of 10%
 314 from 20 ka to 10 ka. The speed changes in the limited ensemble are bimodal: one group shows
 315 speeds at 20 ka between 50% and 90% of the speed at 10 ka. The other group shows between no
 316 change and 10% faster speeds at 20 ka compared to 10 ka. The first group is closer to the speed
 317 that might be expected if the speed was primarily determined by the accumulation rate through a
 318 balance velocity; the second group indicates that dynamic changes are able to counteract the
 319 influence of lower accumulation rates at 20 ka. We thus determine the speeds for ages older than
 320 10.1 ka in two ways: no change in speed and speed changes that scale with an approximate
 321 accumulation history.
 322



323
 324 Figure 7: Histograms of modeled speed changes between 10 ka and 20 ka near South Pole for the
 325 full and limited ensembles (see 2.5 for full description; Pollard et al. 2016)
 326

327
 328 **3.2.1 Segment 1: 0 km to 65 km (0 to 10.1 ka)**

329 The first segment uses the inferred flowline of Lilien et al. (2018). They used a novel method of
330 correlating the SPICEcore layer thicknesses with the geophysically-determined accumulation
331 pattern upstream and found that with a 15% increase in speed from 10.1 ka to today, the
332 upstream pattern of accumulation explained approximately three-quarters of the variance in the
333 SPICEcore accumulation history. Of particular importance to this study, their work tightly
334 constrains the location where the ice in the core was deposited on the surface of the ice sheet.
335 This has not been possible at previous ice-core sites (e.g. WAIS Divide, EDML, NEEM) where
336 ice-flow models provided the only estimates of past velocity.

337
338 The measured velocity field was used to determine the modern flowline. We use the flowline
339 position and age from the preferred scenario of a 15% Holocene speed up of Lilien et al. (2018).
340 The position and age were found by starting at the SPICEcore drill site and recursively stepping
341 upstream in one-year intervals in the direction opposite the velocity vectors to obtain annual
342 positions along the flowline. The velocity direction was fixed in time while the magnitude was
343 linearly decreased to 15% slower velocities at 10.1 ka. The 10.1 ka ice originated 65 km
344 upstream along the flowline.

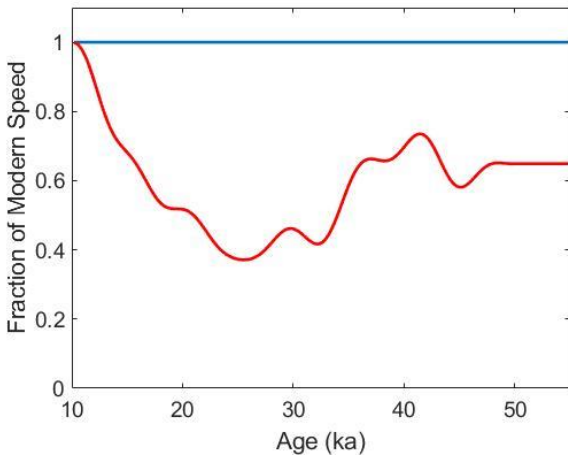
345 346 **3.2.2 Segment 2: 65 to 100 km (10.1 to ~25 ka)**

347 For ice older than 10.1 ka, the spatial variations in the accumulation rate cannot be clearly
348 correlated with the layer thickness variations in SPICEcore. This is likely because: 1) uncertainty
349 in the flowline position increases with distance (age); 2) the relative uncertainty in the surface
350 velocity increases as the velocity decreases with distance upstream; 3) the surface-velocity
351 measurement stakes are farther apart; and 4) the temporal variations in accumulation are likely
352 larger during the isotopic maximum at ~11 ka and the glacial-interglacial transition (Veres et al.,
353 2013; Fudge et al., 2016). This segment of the flowline spans from 65 km to the limit of the
354 surface velocity measurements at 100 km from the SPICEcore drill site. Without the constraints
355 of the correlation analysis, both the flow direction and past ice-flow velocity are much less
356 certain. Continent-scale ice-sheet models have difficulty reproducing the details of ice-flow in
357 the region and are sensitive to boundary forcing assumptions.

358
359 We use two different assumptions about the past ice speed to estimate the flowline position with
360 age before 10.1 ka. For both methods, we start with the inferred speed at 10.1 ka from Lilien et
361 al. (2018; i.e. 15% slower than measured today) and keep the ice-flow direction fixed in time.
362 The first reconstruction assumes that the speed has been constant in time prior to 10.1 ka. The
363 second reconstruction scales the speed to an estimate of the past accumulation rate, essentially
364 assuming that the speed is controlled by the ice flux necessary to keep the ice sheet in balance.

365
366 The speed history used is shown in Figure 8. Winski et al. (2019) only reported the SPICEcore
367 accumulation history for the Holocene (younger than 11.7 ka) because the cumulative thinning
368 layers have experienced becomes increasingly uncertain with depth. Since we are only seeking a
369 plausible estimate of past speed, the increased uncertainty of the thinning function is not a major
370 concern for this work. We obtain an accumulation history for the past 54 ka by dividing the layer
371 thicknesses of the SP19 timescale (Winski et al. 2019) by a thinning function computed with a
372 Dansgaard-Johnson (1969) model of vertical strain with a kink height of 0.2 and low pass filtered
373 at 5 ka. Scaling the ice-flow speed to the accumulation rate results in speeds at the LGM of only

374 40% of modern; thus, ages at the end of the measured flowline, at 100 km from SPICEcore, are 7
375 ka older (28 ka) than with the assumption of a constant speed (21 ka).
376



377
378 Figure 8: Fraction of modern speed used to reconstruction flowline position and age for the
379 constant speed scenario (blue) and scaled to accumulation history (red).
380

381 3.2.3 Segment 3: beyond 100 km (older than ~25 ka)

382 For ice that originated beyond 100 km from SPICEcore, no reliable surface-velocity
383 measurements exist to help define where the ice originated. We examined the utility of the
384 surface topography of BedMap2 (Fretwell et al., 2013) in defining the flow direction by tracking
385 particles along the steepest descent. We computed two flowlines, one going upstream from
386 SPICEcore and the other going downstream from the 10 ka location. They do not agree with
387 each other or with the measured flowline, which is not surprising given the limited data in
388 BedMap2 and the convergent flow. Thus, we do not expect the surface topography to be useful
389 in defining the x and y components of the flowline beyond 100 km and we assume that the ice
390 has flowed in a straight line from an ice divide (Figure 1). The position of the ice divide is not
391 well defined and we assume it is an additional 90 km distant. We also assume that the speed
392 decreases linearly from its value at 100 km to zero at the divide, equivalent to assuming a
393 balance velocity in an ice sheet with uniform ice thickness and accumulation rate and no
394 convergence or divergence, because we have little information of the bedrock topography
395 upstream. We then apply the same two assumptions for the flow speed used for the second
396 segment: either constant speed or varying based on the accumulation history. These assumptions
397 suggest the oldest SPICEcore ice (54.3 ka) originated a total of 135 km to 155 km upstream from
398 SPICEcore.
399

400 3.3 Advection Impact

401 The advection impact on the SPICEcore accumulation-rate and water-isotope histories are quite
402 different from each other. The accumulation rate is sampled with high frequency but shows no
403 long-term trend with distance and elevation. The water isotopes, on the other hand, are sampled
404 infrequently but show a linear trend with distance and elevation. We discuss the advection
405 impact for the two separately.
406

407 3.3.1 Accumulation Rate

408 The lack of a linear trend in the accumulation rate along the flowline indicates that no trend
409 should be removed from the SPICEcore accumulation history. However, the variation in
410 accumulation upstream has a major impact on the SPICEcore history. Lilien et al. (2018) were
411 able to isolate the influence of km-scale upstream variability for the past 10 ka, which explains a
412 majority of the variance in the SPICEcore accumulation history. Thus, little of the variability in
413 the accumulation history for the past 10 ka is due to climate. While the residual variance of the
414 SPICEcore accumulation history (the accumulation history after removing the advection impact)
415 might reflect temporal changes in climate, the residual variance is also affected by multiple
416 sources of uncertainty such as the assumptions of a constant spatial pattern of accumulation, a
417 fixed flowline, a linear speed up, and a spatially homogeneous firn-density profile. These
418 uncertainties are sufficiently large and difficult to quantify that we do not interpret the residual as
419 a temporal history of accumulation.

420
421 Beyond 10 ka, it is important to understand the potential influences of spatial variations in
422 accumulation in order to avoid erroneous conclusions about temporal variations in the
423 accumulation rate over the past 54 ka. Since there is no overall trend, we are primarily interested
424 in how the spatial variability could be imprinted in the ice-core history. Spectral analysis of the
425 spatial pattern of accumulation shows that there is significant power at a wavelength of 5 to 10
426 km. The temporal imprint of the spatial variations on ice-core derived accumulation rates is then
427 determined by the ice-flow velocity, which is 4 m a^{-1} for ice of 10 ka age and decreases to 1 m a^{-1}
428 for ice of 54 ka age. The timescales affected in the accumulation history are ~ 1 to 6 ka during the
429 deglacial transition (10-20 ka) and get longer, reaching 10 ka, for the glacial SPICEcore ice. The
430 advection impact on the deglacial transition may affect the specific timing of accumulation-rate
431 change, but not the overall temporal trend. For older ages, the advection impact has a similar
432 timescale to millennial-scale climate variations. We thus expect that the advection impact will
433 decrease the coherence between the accumulation-rate history and the temperature history
434 inferred from water isotopes.

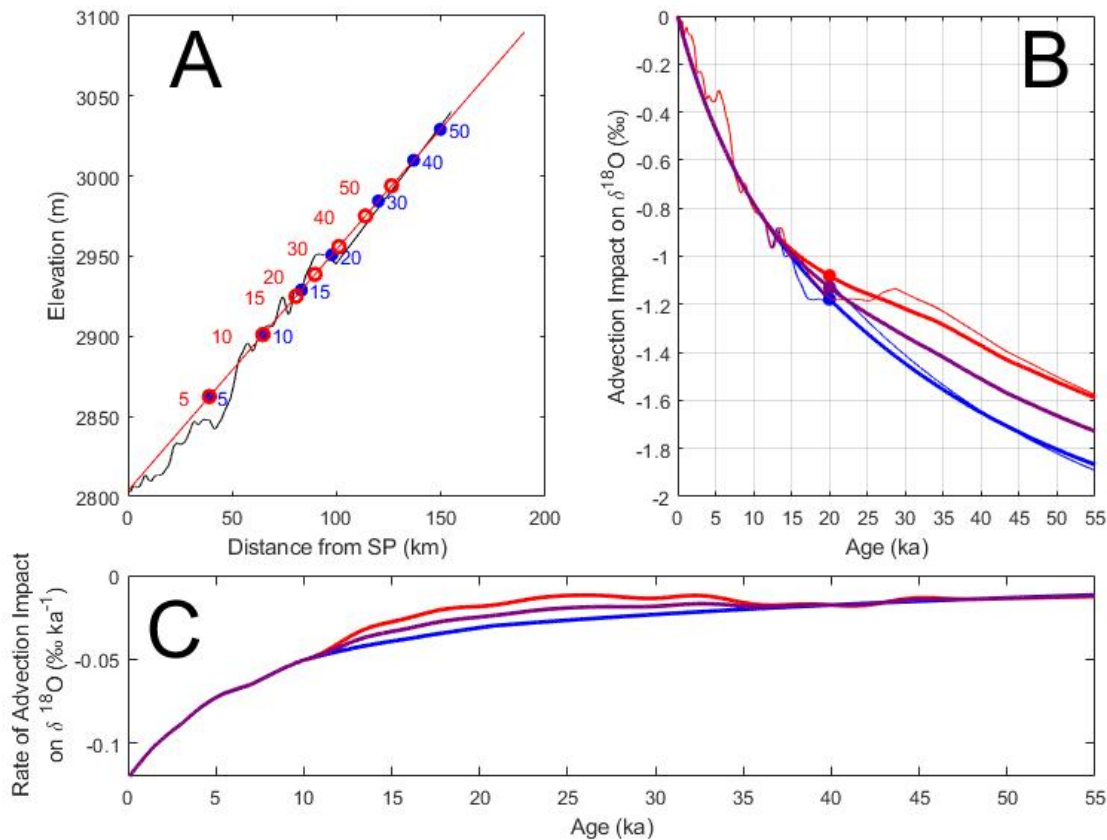
435 436 **3.3.2 Water Isotopes**

437 The water isotopes are not sampled at a high enough spatial resolution to perform an analysis of
438 millennial-scale variations as was done for the accumulation rate; however, the $\delta^{18}\text{O}$ and δD both
439 show linear trends with elevation and distance. Because $\delta^{18}\text{O}$ and δD are similar, we will discuss
440 only the advection correction for $\delta^{18}\text{O}$ in this section (both are provided in the supplemental
441 spreadsheet). A correction for advection becomes important, particularly for questions such as
442 the magnitude of the glacial-interglacial temperature change. We use a linear fit to elevation data
443 as the base for the advection correction (Figure 9). The linear fit is continued beyond 100 km at
444 the same slope, reaching an elevation similar to the US-ITASE 07-04 core at 190 km upstream of
445 SPICEcore. We use the linear fit to avoid meter-scale elevation variability being added through
446 the advection correction.

447
448 We use the two inferences of the origin positions of ice in SPICEcore described in section 3.2 to
449 find the elevation change through time due to advection. We convert this into an advection
450 impact for $\delta^{18}\text{O}$ based on the linear $\delta^{18}\text{O}$ -elevation fit (Section 3.1.2; Figure 5), which we assume
451 is constant in time. The two scenarios provide an estimate of the range of plausible advection
452 impacts. While we do not have enough information to define a formal uncertainty on the
453 advection impact, the difference between the two scenarios provides a qualitative uncertainty

454 estimate for the effect of past speed changes. We use the average of these two scenarios as our
455 best estimate of the advection impact and report all three in the supplementary table.

456
457 SPICEcore ice of 20 ka age is approximately 1.1‰ more enriched than if it had fallen at South
458 Pole instead of at ~95 km upstream and at ~135 m higher elevation. The uncertainty of this
459 advection impact due to the temporal surface velocity assumption is approximately $\pm 0.1\%$;
460 however, there is additional uncertainty due to the slope of the elevation-water isotope fit.
461 Because the elevation change is linear with distance, the curvature of the advection impact is
462 determined by the change in ice velocity and the advection impact increases the most rapidly at
463 the youngest ages. The difference over the Holocene (past 11.7 ka) is 0.85‰ while the additional
464 difference to the LGM (20 ka) is only 0.25‰. The advection impact for the oldest ice is only
465 about 0.01‰ per ka and is nearly the same for both velocity assumptions after 35 ka; this is
466 because the ice in the constant-speed scenario has moved closer to the divide where the speed is
467 lower and thus is similar to the lower speed in the accumulation-scaled scenario.
468



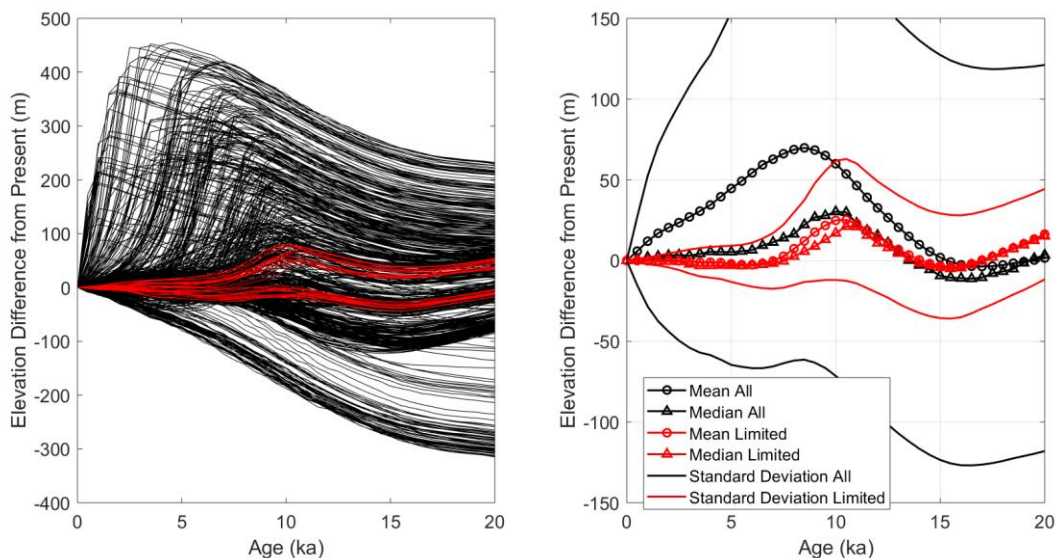
469
470 Figure 9: Advection Impact for $\delta^{18}\text{O}$. A): Elevation profile (black) and linear fit (red) used in
471 advection correction. Elevations at 5 ka intervals for the constant velocity assumption (blue dots)
472 and scale to accumulation history (red circles). B): Advection correction using elevations in left
473 panel. Blue is constant velocity. Red is scaled to accumulation history. Thick lines use linear
474 elevation change; thin lines use measured elevation along flowline. The average of the two
475 assumptions is shown in purple. A negative value indicates the ice recovered in the core fell at a

476 location where the water isotopes are more depleted than South Pole in the current climate. C)
477 The rate of the advection impact for the three curves in the upper right panel.
478

479 **3.4 Ice Sheet Elevation Change**

480 The in situ measurements performed in this study provide little in the way of constraints for past
481 ice thickness change. Lilien et al. (2018) noted that the inferred 15% Holocene speed up could be
482 caused by either a modest thickening of ~100 m or a steeping of a few percent. However, the
483 analysis cannot be used for older ages with larger climate changes and potentially more elevation
484 change. Therefore, we assess the range of plausible elevation change using the output of a 625-
485 member ensemble of a full ice-sheet model (Pollard et al., 2016) as well as a limited ensemble
486 (32 members) of the most likely parameter combinations (see section 2.5). We calculate the
487 mean, median, and standard deviation of the elevation change relative to modern (Figure 10) for
488 the full and limited ensembles. We note that every member of the limited ensemble has ice
489 thickness changes of less than 100 m in past 10 ka.
490

491 The full ensemble suggests the ice sheet thickened, and the surface elevation increased, from
492 15ka to 8 ka, before Holocene thinning reduced the ice sheet elevation back to near 20 ka values.
493 The median change is roughly half the magnitude of the mean with a peak elevation that occurs
494 at about 10 ka. The limited ensemble shows limited variance about the full model median, with
495 less elevation change after 8 ka and a slightly higher elevation at 20 ka. The limited ensemble is
496 bimodal, with the group of runs with a higher elevation at 10 ka corresponding to the basal
497 sliding coefficient of ungrounded areas parameter (CSHELF) equal to -6 and the group of runs
498 with lower elevations at 10 ka from runs with CSHELF equal to -5. The maximum elevation
499 change of the limited ensemble mean is +26 m at 10 ka. The mean elevation is +16 m at 20 ka. In
500 all cases, one standard deviation encompasses both higher and lower elevations for all past ages
501 to 20 ka. Therefore, we do not provide an explicit correction for past ice sheet elevation. An
502 elevation change of 26 m corresponds to a 0.2 ‰ impact for $\delta^{18}\text{O}$ using the measured, modern,
503 spatial slope of 0.008 ‰ m^{-1} . This is roughly one quarter of the advection correction at 10 ka.
504 Thus, uncertainty from possible ice sheet elevation change should be considered in any
505 interpretation of the water isotope record, but existing ice-sheet models cannot sufficiently
506 constrain the elevation history to warrant an explicit correction.
507



508
 509 Figure 10: Left Panel: Elevation difference from modern for each model run in the Pollard et al.
 510 2016 ensemble (black, 625 members) and limited ensemble (red, 32 members) of the most likely
 511 parameter combinations. Right panel: mean (circles), median (triangles), and standard deviation
 512 (thin lines) of full ensemble (black) and limited ensemble (red).

513
 514 **4 Discussion**

515 Advection has enhanced the glacial-interglacial $\delta^{18}\text{O}$ change at SPICEcore by $\sim 1\text{‰}$ because ice
 516 in the core originated at higher elevations with more depleted isotopic values. The total LGM (20
 517 ka) to modern (past 1 ka) $\delta^{18}\text{O}$ change in SPICEcore is approximately 6‰ (Kahle et al., 2018).
 518 Accounting for advection reduces the fixed-location glacial-interglacial change to 5‰ .
 519 Advection has the opposite impact at the WAIS Divide ice core (WDC), where advection
 520 increases the glacial-interglacial change by 1‰ to 8‰ (Steig et al., 2013; WAIS Divide Project
 521 Members, 2013). Understanding the advection impact is important for comparing the magnitude
 522 of isotopic change among Antarctic ice cores; WDC has a 1‰ greater LGM-modern change than
 523 SPICEcore in the measured records, but a 3‰ greater change after accounting for advection.
 524 Because SPICEcore and WDC have similar source regions and distillation pathways (e.g.
 525 Sodemann and Stohl, 2009), the difference between the two cores has the potential to yield
 526 insight into the relative elevation change between the West and East Antarctic ice sheets and to
 527 further refine the range of plausible model results presented in Figure 10. A full interpretation of
 528 relative isotopic change between SPICEcore and WDC is beyond the scope of this paper, but
 529 including the impact of advection is critical for future analysis.

530
 531 The advection impact on the accumulation history is distinct from that for the water isotopes.
 532 There is no linear trend in accumulation in the upstream catchment, and thus no trend to remove
 533 from the SPICEcore accumulation history. High spatial resolution measurements of the modern
 534 upstream accumulation pattern have revealed that the majority of the accumulation variability in
 535 the past 10 ka is caused by advection and not temporal changes (Lilien et al., 2018). While the
 536 upstream pattern and SPICEcore history cannot be correlated for ages older than 10 ka, the
 537 spatial pattern is still expected to impact the accumulation history. The dominant timescales
 538 affected increase from ~ 1 ka in the Holocene to ~ 10 ka at 50 ka. These timescales are similar to

539 that of millennial climate change and thus we expect the spatial variability of accumulation that
540 is imprinted on the SPICEcore temporal history to decrease the coherence between water isotope
541 (as a proxy for temperature) and accumulation records. Overall, changes in accumulation of less
542 than 20% on millennial timescales should not be interpreted as a climate signal.

543
544 The different character of the advection impacts for water isotopes and accumulation arise
545 because there is no coherent relationship between water isotopes and accumulation rate. This
546 may be because the water isotopes are largely controlled by the condensation temperature
547 (Jouzel et al., 1997), whereas the accumulation rate is affected by wind redistribution and the
548 local surface topography (Hamilton, 2004). In fact, the curvature (second derivative) of the
549 elevation profile along the flowline explains a third of the variance in the modern spatial pattern
550 of accumulation, similar to areas in Greenland (Miege et al., 2013; Hawley et al., 2014).

551
552 The impact of elevation change on the isotopic records is not clear. An ensemble of continental-
553 scale ice sheet model runs showed minimal mean and median elevation changes in the past. The
554 standard deviation of the runs always included changes of both signs. Therefore we do not
555 suggest a correction for ice-sheet elevation change through time but note that there is uncertainty
556 associated with a possible change that should be considered in subsequent analyses. We also
557 could not determine the temperature lapse rate from our 10 m borehole temperatures; however,
558 we can estimate the temperature impact of advection based on a dry adiabatic lapse rate of 10°C
559 km^{-1} , which is consistent with our measurements. The LGM ice fell at ~ 140 m higher elevation
560 and likely would be $\sim 1.4^{\circ}\text{C}$ colder than if it had fallen at the current elevation of South Pole.

561 562 **5 Conclusion**

563 The relatively fast ice speed at South Pole today causes ice at depth in SPICEcore to have
564 originated at locations up to 155 km away in the direction of Titan Dome and at elevations
565 upstream of up to 230 m higher, assuming the ice-sheet configuration has not changed
566 significantly in the past. Elevation change of the ice sheet through time is likely small and of
567 uncertain sign. Our measurements in the upstream catchment define the flow direction and speed
568 as well as spatial gradients in the accumulation rate and water isotopes. These measurements
569 identify the impact of advection on the SPICEcore records. The accumulation rate has no spatial
570 trend, but shows 20% variations on length scales of 5-10 km; $\delta^{18}\text{O}$ shows a -0.008‰ m^{-1}
571 depletion which enhances the measured LGM-Holocene change in the ice core by $\sim 1\text{‰}$. This
572 work facilitates accurate interpretation of the SPICEcore records as temporal histories of climate
573 at South Pole.

574 575 **6 Data Availability**

576 Velocity and radar data are available at <http://www.usap-dc.org/view/dataset/601100>. Water
577 isotope, accumulation rate, and advection corrections will be posted upon acceptance.

578 579 **7 Author Contributions**

580 All authors contributed to the analysis and writing of the manuscript. HC, DL, MS, and MK
581 performed the field work. AS, TF, and ES performed water isotope analysis. TF, NH, and ES
582 analyzed the ice-sheet model ensemble.

583 584 **8 Competing Interests**

585 The authors declare no competing interests.

586

587 **9 Acknowledgements**

588 This work was funded through U.S. National Science Foundation grants 1443471 and 1443232
589 (MK, EW, HC, TJF); 1443105 and 141839 (EJS). We thank the Ice Drill Program Office for
590 recovering the ice core; the 109th New York Air National Guard for airlift in Antarctica;
591 Elizabeth Morton, David Clemens-Sewall, Maurice Conway, Mike Waskiewicz for their efforts
592 in the field; Antarctic Support Contractors and the members of South Pole station who facilitated
593 the field operations; UNAVCO for power supplies and GPS support; and the National Science
594 Foundation Ice Core Facility for ice-core processing.

595

596 **References**

- 597 Alley, R.B., Meese, D.A., Shuman, C.A., Gow, A.J., Taylor, K.C., Grootes, P.M., White, J.W.C.,
598 Ram, M., Waddington, E.D., Mayewski, P.A., and Zielinski, G.A.: Abrupt increase in
599 greenland snow accumulation at the end of the younger dryas event. *Nature*, **362**(6420): 527-
600 529, 1993.
- 601 Briggs, R.D., Pollard, D. and Tarasov, L.: A data-constrained large ensemble analysis of
602 Antarctic evolution since the Eemian. *Quaternary Science Reviews*, **103**: 91-115, 2014
- 603 Casey, K.A., Fudge, T.J., Neumann, T.A., Steig, E.J., Cavitte, M.G.P. and Blankenship, D.D.:
604 The 1500 m South Pole ice core: recovering a 40 ka environmental record. *Annals of*
605 *Glaciology*, **55**(68): 137-146, 2014
- 606 Cuffey, K.M. and Clow, G.D.: Temperature, accumulation, and ice sheet elevation in central
607 Greenland through the last deglacial transition. *Journal of Geophysical Research-Oceans*,
608 **102**(C12): 26383-26396, 1997
- 609 Cuffey, K.M. and Paterson, W.S.B.: *The Physics of Glaciers*. Fourth Edition. 2010
- 610 Dansgaard, W., Johnsen, S.J., Moller, J., Langway Jr., C.C.: One thousand centuries of climatic
611 record from Camp Century on the Greenland Ice Sheet, *Science*, 166, 3903, 377-380, 1969
- 612 DeConto, R.M. and Pollard, D.: Contribution of Antarctica to past and future sea-level rise.
613 *Nature*, **531**(7596): 591-597, 2016
- 614 Dixon, D.A., Mayewski, P.A., Korotkikh, E., Sneed, S.B., Handley, M.J., Introne, D.S. and
615 Scambos, T.A.: Variations in snow and firn chemistry along US ITASE traverses and the
616 effect of surface glazing. *Cryosphere*, **7**(2): 515-535, 2013
- 617 EPICA, Augustin, L., Barbante, C., Barnes, PRF., Barnola, JM., Bigler, M., Castellano, E.,
618 Cattani, O., Chappellaz, J., DahlJensen, D., Delmonte, B., Dreyfus, G., Durand, G., Falourd,
619 S., Fischer, H., Fluckiger, J., Hansson, M.E., Huybrechts, P., Jugie, R., Johnsen, S.J., Jouzel,
620 J., Kaufmann, P., Kipfstuhl, J., Lambert, F., Lipenkov, V.Y., Littot, G.V.C., Longinelli, A.,
621 Lorrain, R., Maggi, V., Masson-Delmotte, V., Miller, H., Mulvaney, R., Oerlemans, J.,
622 Oerter, H., Orombelli, G., Parrenin, .,F Peel, D.A., Petit, J.R., Raynaud, D., Ritz, C., Ruth,
623 U., Schwander, J., Siegenthaler, U., Souchez, R., Stauffer, B., Steffensen, J.P., Stenni, B.,
624 Stocker, T.F., Tabacco, I.E., Udisti, R., van de Wal, R.S.W., van den Broeke, M., Weiss, J.,
625 Wilhelms, F., Winther, J.G., Wolff, E.W., Zucchelli, M.: One-to-one coupling of glacial
626 climate variability in Greenland and Antarctica. *Nature*, **444**(7116): 195-198, 2006
- 627 Ferris, D. G., J. Cole-Dai, A. R. Reyes, and D. M. Budner, 2011, South Pole ice core record of
628 explosive volcanic eruptions in the first and second millennia A.D. and evidence of a large
629 eruption in the tropics around 535 A.D., *J. Geophys. Res.*, 116, D17308,
630 doi:10.1029/2011JD015916.

631 Fretwell, P., Pritchard, H.D., Vaughan, D.G., Bamber, J.L., Barrand, N.E., Bell, R., Bianchi, C.,
632 Bingham, R.G., Blankenship, D.D., Casassa, G., Catania, G., Callens, D., Conway, H., Cook,
633 A.J., Corr, H.F.J., Damaske, D., Damm, V., Ferraccioli, F., Forsberg, R., Fujita, S., Gim, Y.,
634 Gogineni, P., Griggs, J.A., Hindmarsh, R.C.A., Holmlund, P., Holt, J.W., Jacobel, R.W.,
635 Jenkins, A., Jokat, W., Jordan, T., King, E.C., Kohler, J., Krabill, W., Riger-Kusk, M.,
636 Langley, K.A., Leitchenkov, G., Leuschen, C., Luyendyk, B.P., Matsuoka, K., Mouginot, J.
637 Nitsche, F.O., Nogi, Y., Nost, O.A., Popov, S.V., Rignot, E., Ripplin, D.M., Rivera, A.,
638 Roberts, J., Ross, N., Siegert, M.J., Smith, A.M., Steinhage, D., Studinger, M., Sun, B.,
639 Tinto, B.K., Welch, B.C., Wilson, D., Young, D.A., Xiangbin, C. and Zirizzotti, A.:
640 Bedmap2: improved ice bed, surface and thickness datasets for Antarctica. *Cryosphere*, **7**(1):
641 375-393, 2013

642 Fudge, T.J., Markle, B.R., Cuffey, K.M., Buizert, C., Taylor, K.C., Steig, E.J., Waddington,
643 E.D., Conway, H. and Koutnik, M.: Variable relationship between accumulation and
644 temperature in West Antarctica for the past 31,000 years. *Geophysical Research Letters*,
645 **43**(8): 3795-3803, 2016

646 Golledge, N.R., Menviel, L., Carter, L., Fogwill, C.J., England, M.H., Cortese G., and Levy,
647 R.H.: Antarctic contribution to meltwater pulse 1A from reduced Southern Ocean
648 overturning. *Nature Communications*, **5**, 2014

649 Gow, A.J., Ueda, H.T. and Garfield, D.E.: Antarctic ice sheet - preliminary results of first core
650 hole to bedrock. *Science*, **161**(3845): 1011-1014, 1968.

651 Hamilton, G.S. 2004. Topographic control of regional accumulation rate variability at South Pole
652 and implications for ice-core interpretation. *Annals of Glaciology, Vol 39, 2005*, **39**: 214-218.

653 Hammer, C.U., Clausen, H.B., and Dansgaard, W.: Greenland ice-sheet evidence of post-glacial
654 volcanism and its climatic impact. *Nature*, **288**(5788): 230-235, 1980

655 Hawley, R.L., Courville, Z.R., Kehrl, L.M., Lutz, E.R., Osterberg, E.C.T., Overly, B. and Wong,
656 G.J.: Recent accumulation variability in northwest Greenland from ground-penetrating radar
657 and shallow cores along the Greenland Inland Traverse. *Journal of Glaciology*, **60**(220): 375-
658 382, 2014

659 Huybrechts, P., Rybak, O., Pattyn, F., Ruth, U. and Steinhage, D.: Ice thinning, upstream
660 advection, and non-climatic biases for the upper 89% of the EDML ice core from a nested
661 model of the Antarctic ice sheet. *Climate of the Past*, **3**(4): 577-589, 2007

662 Jouzel, J., Alley, R.B., Cuffey, K.M., Dansgaard, W., Grootes, P., Hoffmann, G., Johnsen, S.J.,
663 Koster, R.D., Peel, D., Shuman, C.A., Stievenard, M., Stuiver M., and White, J.: Validity of
664 the temperature reconstruction from water isotopes in ice cores. *Journal of Geophysical*
665 *Research-Oceans*, **102**(C12): 26471-26487, 1997

666 Kahle, E. C., Holme, C., Jones, T. R., Gkinis, V., & Steig, E. J. (2018). A generalized approach
667 to estimating diffusion length of stable water isotopes from ice-core data. *Journal of*
668 *Geophysical Research: Earth Surface*, **123**, 2377–2391.
669 <https://doi.org/10.1029/2018JF004764>

670 Koutnik, M.R., Fudge, T.J., Conway, H., Waddington, E.D., Neumann, T.A., Cuffey, K.M.,
671 Buizert, C., and Taylor, K.C.: Holocene accumulation and ice flow near the West Antarctic
672 Ice Sheet Divide ice core site. *Journal of Geophysical Research-Earth Surface*, **121**(5): 907-
673 924, 2016

674 Lilien, D.A., Fudge, T.J., Koutnik, M.R., Conway, H., Osterberg, E.C., Ferris, D.G.,
675 Waddington, E.D. and Stevens, C.M.: Holocene Ice-Flow Speedup in the Vicinity of the
676 South Pole. *Geophysical Research Letters*, **45**(13): 6557-6565: 2018

677 Lorius, C., Jouzel, J., Ritz, C., Merlivat, L., Barkov, N.I., Korotkevich, Y.S. and Kotlyakov,
678 V.M.: A 150,000-year climatic record from antarctic ice. *Nature*, **316**(6029): 591-596, 1985
679 Marcott, S.A., Bauska, T.K., Buizert, C., Steig, E.J., Rosen, J.L., Cuffey, K.M., Fudge, T.J.,
680 Severinghaus, J.P., Ahn, J., Kalk, M.L., McConnell, J.R., Sowers, T., Taylor, K.C., White,
681 J.W.C., and Brook, E.J.: Centennial-scale changes in the global carbon cycle during the last
682 deglaciation. *Nature*, **514**(7524): 616-620, 2014
683 Markle, B.R., Steig, E.J., Buizert, C., Schoenemann, S.W., Bitz, C.M., Fudge, T.J., Pedro, J.B.,
684 Ding, Q.H., Jones, T.R., White, J.C. and Sowers, T. Global atmospheric teleconnections
685 during Dansgaard-Oeschger events. *Nature Geoscience*, **10**(1): 36-40, 2017
686 Martinerie, P., Lipenkov, V.Y., Raynaud, D., Chappellaz, J., Barkov, N.I. and Lorius, C.: Air
687 content paleo record in the vostok ice core (antarctica) - a mixed record of climatic and
688 glaciological parameters. *Journal of Geophysical Research-Atmospheres*, **99**(D5): 10565-
689 10576, 1994
690 Masson-Delmotte, V., Hou, S., Ekaykin, A., Jouzel, J., Aristarain, A., Bernardo, R.T.,
691 Bromwich, D., Cattani, O., Delmotte, M., Falourd, S., Frezzotti, M., Gallee, H., Genoni, L.,
692 Isaksson, E., Landais, A., Helsen, M.M., Hoffmann, G., Lopez, J., Morgan, V., Motoyama,
693 H., Noone, D., Oerter, H., Petit, J.R., Royer, A., Uemura, R., Schmidt, G.A., Schlosser, E.,
694 Simoes, J.C., Steig, E.J., Stenni, B., Stievenard, M., van den Broeke, M.R., de Wal, R., de
695 Berg, W.J.V., Vimeux, F. and White, J.W.C.: A review of Antarctic surface snow isotopic
696 composition: Observations, atmospheric circulation, and isotopic modeling. *Journal of*
697 *Climate*, **21**(13): 3359-3387, 2008
698 Miege, C., Forster, R.R., Box, J.E., Burgess, E.W., McConnell, J.R., Pasteris, D.R. and Spikes,
699 V.B.: Southeast Greenland high accumulation rates derived from firn cores and ground-
700 penetrating radar. *Annals of Glaciology*, **54**(63): 322-332, 2013
701 Morse, D.L., Blankenship, D.D., Waddington, E.D. and Neumann, T.A. A site for deep ice
702 coring in West Antarctica: results from aerogeophysical surveys and thermo-kinematic
703 modeling. *Annals of Glaciology, Vol 35*, **35**: 36-44, 2002
704 NEEM, Dahl-Jensen, D., Albert, M. R., Aldahan, A., Azuma, N., Balslev-Clausen, D.,
705 Baumgartner, M., Berggren, A. -M., Bigler, M., Binder, T., Blunier, T., Bourgeois, J. C.,
706 Brook, E. J., Buchardt, S. L., Buizert, C., Capron, E., Chappellaz, J., Chung, J., Clausen, H.
707 B., Cvijanovic, I., Davies, S. M., Ditlevsen, P., Eicher, O., Fischer, H., Fisher, D. A., Fleet,
708 L. G., Gfeller, G., Gkinis, V., Gogineni, S., Goto-Azuma, K., Grinsted, A., Gudlaugsdottir,
709 H., Guillevic, M., Hansen, S. B., Hansson, M., Hirabayashi, M., Hong, S., Hur, S. D.,
710 Huybrechts, P., Hvidberg, C. S., Iizuka, Y., Jenk, T., Johnsen, S. J., Jones, T. R., Jouzel, J.,
711 Karlsson, N. B., Kawamura, K., Keegan, K., Kettner, E., Kipfstuhl, S., Kjaer, H. A., Koutnik,
712 M., Kuramoto, T., Koehler, P., Laepple, T., Landais, A., Langen, P. L., Larsen, L. B.,
713 Leuenberger, D., Leuenberger, M., Leuschen, C., Li, J., Lipenkov, V., Martinerie, P.,
714 Maselli, O. J., Masson-Delmotte, V., McConnell, J. R., Miller, H., Mini, O., Miyamoto, A.,
715 Montagnat-Rentier, M., Mulvaney, R., Muscheler, R., Orsi, A. J., Paden, J., Panton, C.,
716 Pattyn, F., Petit, J. -R., Pol, K., Popp, T., Possnert, G., Prie, F., Prokopiou, M., Quiquet, A.,
717 Rasmussen, S. O., Raynaud, D., Ren, J., Reutenauer, C., Ritz, C., Rockmann, T., Rosen, J.
718 L., Rubino, M., Rybak, O., Samyn, D., Sapart, C. J., Schilt, A., Schmidt, A. M. Z.,
719 Schwander, J., Schuepbach, S., Seierstad, I., Severinghaus, J. P., Sheldon, S., Simonsen, S.
720 B., Sjolte, J., Solgaard, A. M., Sowers, T., Sperlich, P., Steen-Larsen, H. C., Steffen, K.,
721 Steffensen, J. P., Steinhage, D., Stocker, T. F., Stowasser, C., Sturevik, A. S., Sturges, W. T.,
722 Sveinbjornsdottir, A., Svensson, A., Tison, J. -L., Uetake, J., Vallelonga, P., van de Wal, R.

723 S. W., van der Wel, G., Vaughn, B. H., Vinther, B., Waddington, E., Wegner, A., Weikusat,
724 I., White, J. W. C., Wilhelms, F., Winstrup, M., Witrant, E., Wolff, E. W., Xiao, C., Zheng,
725 J.: Eemian interglacial reconstructed from a Greenland folded ice core. *Nature*, **493**(7433):
726 489-494, 2013

727 NorthGRIP, Andersen, K.K., Azuma, N., Barnola, J.M., Bigler, M., Biscaye, P., Caillon, N.,
728 Chappellaz, J., Clausen, H.B., DahlJensen, D., Fischer, H., Fluckiger, J., Fritzsche, D., Fujii,
729 Y., Goto-Azuma, K., Gronvold, K., Gundestrup, N.S., Hansson, M., Huber, C., Hvidberg,
730 C.S., Johnsen, S.J., Jonsell, U., Jouzel, J., Kipfstuhl, S., Landais, A., Leuenberger, M.,
731 Lorrain, R., Masson-Delmotte, V., Miller, H., Motoyama, H., Narita, H., Popp, T.,
732 Rasmussen, S.O., Raynaud, D., Rothlisberger, R., Ruth, U., Samyn, D., Schwander, J., Shoji,
733 H., Siggard-Andersen, M.L., Steffensen, J.P., Stocker, T., Sveinbjornsdottir, A.E., Svensson,
734 A., Takata, M., Tison, J.L., Thorsteinsson, T., Watanabe, O., Wilhelms, F., White, J.W.C.:
735 High-resolution record of Northern Hemisphere climate extending into the last interglacial
736 period. *Nature*, **431**(7005): 147-151, 2004

737 Parrenin, F., Dreyfus, G., Durand, G., Fujita, S., Gagliardini, O., Gillet, F., Jouzel, J., Kawamura,
738 K., Lhomme, N., Masson-Delmotte, V., Ritz, C., Schwander, J., Shoji, H., Uemura, R.,
739 Watanabe, O. and Yoshida, N. 1-D-ice flow modelling at EPICA Dome C and Dome Fuji,
740 East Antarctica. *Climate of the Past*, **3**(2): 243-259, 2007

741 Petit, J.R., Jouzel, J., Raynaud, D., Barkov, N.I., Barnola, J.M., Basile, I., Bender, M.,
742 Chappellaz, J., Davis, M., Delaygue, G., Delmotte, M., Kotlyakov, V.M., Legrand, M.,
743 Lipenkov, V.Y., Lorius, C., Pepin, L., Ritz, C., Saltzman, E. and Stievenard, M.: Climate and
744 atmospheric history of the past 420,000 years from the Vostok ice core, Antarctica. *Nature*,
745 **399**(6735): 429-436, 1999

746 Pollard, D. and R. DeConto, 2012. Description of a hybrid ice sheet-shelf model and application
747 to Antarctica, *Geosci. Model Dev.*, **5**, 1273–1295, [www.geosci-model-](http://www.geosci-model-dev.net/5/1273/2012/doi:10.5194/gmd-5-1273-2012)
748 [dev.net/5/1273/2012/doi:10.5194/gmd-5-1273-2012](http://www.geosci-model-dev.net/5/1273/2012/doi:10.5194/gmd-5-1273-2012)

749 Pollard, D., W. Chang, M. haran, P. Applegate, R. DeConto, 2016. Large ensemble modeling of
750 the last deglacial retreat of the West Antarctic ice sheet: comparison of simple and advanced
751 statistical techniques, *Geoscience Model Development*, **9**, 1697–1723, [www.geosci-model-](http://www.geosci-model-dev.net/9/1697/2016/doi:10.5194/gmd-9-1697-2016)
752 [dev.net/9/1697/2016/doi:10.5194/gmd-9-1697-2016](http://www.geosci-model-dev.net/9/1697/2016/doi:10.5194/gmd-9-1697-2016)

753 Price, S.F., Conway, H., and Waddington, E.D.: Evidence for late pleistocene thinning of Siple
754 Dome, West Antarctica. *Journal of Geophysical Research-Earth Surface*, **112**(F3), 2007

755 Rignot, E., Mouginot, J., and Scheuchl, B.: Ice Flow of the Antarctic Ice Sheet. *Science*,
756 **333**(6048): 1427-1430, 2011

757 Severinghaus, J.P., Grachev, A. and Battle, M.: Thermal fractionation of air in polar firn by
758 seasonal temperature gradients. *Geochemistry Geophysics Geosystems*, **2**, 2001

759 Sodemann, H. and Stohl, A.: Asymmetries in the moisture origin of Antarctic precipitation.
760 *Geophysical Research Letters*, **36**, 2009

761 Steig, E.J., Ding, Q., White, J.W.C., Kuttel, M., Rupper, S.B., Neumann, T.A., Neff, P.D.,
762 Gallant, A.J.E., Mayewski, P.A., Taylor, K.C., Hoffmann, G., Dixon, D.A., Schoenemann,
763 S.W., Markle, B.R., Fudge, T.J., Schneider, D.P., Teel, R.P., Vaughn, B.H., Burgener, L.,
764 Williams, J., and Korotkikh, E.: Recent climate and ice-sheet changes in West Antarctica
765 compared with the past 2,000 years. *Nature Geoscience*, **6**: 372-375, 2013

766 Steig, E.J., Fastook, J.L., Zweck, C., Goodwin, I.D., Licht, K., White, J.W.C. and Ackert, R.P.:
767 West Antarctic ice-sheet elevation changes. In *Environment of the West Antarctic Ice Sheet*,
768 *ed. R. Alley and R. Bindshadler*, Antarctic Research Series, 75-90, 2001

769 Steig, E.J., Kahle, E., Jones, T., Morris, V., Vaughn, B., and White, J., in prep., The SPICEcore-
770 triple-isotope record.

771 Stenni, B., Buiron, D., Frezzotti, M., Albani, S., Barbante, C., Bard, E., Barnola, J.M., Baroni,
772 M., Baumgartner, M., Bonazza, M., Capron, E., Castellano, E., Chappellaz, J., Delmonte, B.,
773 Falourd, S., Genoni, L., Iacumin, P., Jouzel, J., Kipfstuhl, S., Landais, A., Lemieux-Dudon,
774 B., Maggi, V., Masson-Delmotte, V., Mazzola, C., Minster, B., Montagnat, M., Mulvaney,
775 R., Narcisi, B., Oerter, H., Parrenin, F., Petit, J.R., Ritz, C., Scarchilli, C., Schilt, A.,
776 Schupbach, S., Schwander, J., Selmo, E., Severi, M., Stocker, T.F. and Udisti, R.: Expression
777 of the bipolar see-saw in Antarctic climate records during the last deglaciation. *Nature*
778 *Geoscience*, **4**(1): 46-49, 2011

779 Van der Veen, C.J., E. Mosley-Thompson, A.J. Gow, B.G. Mark, 1999. Accumulation at South
780 Pole: comparison of two 900-year records, *Geophysical Research Letters*, 104(D24), 31067-
781 31076.

782 Veres, D., Bazin, L., Landais, A., Kele, H.T.M., Lemieux-Dudon, B., Parrenin, F., Martinerie, P.,
783 Blayo, E., Blunier, T., Capron, E., Chappellaz, J., Rasmussen, S.O., Severi, M., Svensson,
784 A., Vinther, B., and Wolff, E.W.: The Antarctic ice core chronology (AICC2012): an
785 optimized multi-parameter and multi-site dating approach for the last 120 thousand years.
786 *Climate of the Past*, **9**(4): 1733-1748, 2013

787 Vinther, B.M., Buchardt, S.L., Clausen, H.B., Dahl-Jensen, D., Johnsen, S.J., Fisher, D.A.,
788 Koerner, R.M., Raynaud, D., Lipenkov, V., Andersen, K.K., Blunier, T., Rasmussen, S.O.,
789 Steffensen, J.P. and Svensson, A.M.: Holocene thinning of the Greenland ice sheet. *Nature*,
790 **461**(7262): 385-388, 2009

791 Waddington, E.D., Bolzan, J.F. and Alley, R.B.: Potential for stratigraphic folding near ice-sheet
792 centers. *Journal of Glaciology*, **47**(159): 639-648, 2001

793 Waddington, E.D., Conway, H., Steig, E.J., Alley, R.B., Brook, E.J., Taylor, K.C. and White,
794 J.W.C.: Decoding the dipstick: Thickness of Siple Dome, West Antarctica, at the Last Glacial
795 Maximum. *Geology*, **33**(4): 281-284, 2005

796 Waddington, E.D., Neumann, T.A., Koutnik, M.R., Marshall, H.P., and Morse, D.L.: Inference
797 of accumulation-rate patterns from deep layers in glaciers and ice sheets. *Journal of*
798 *Glaciology*, **53**(183): 694-712, 2007

799 WAIS Divide Project Members, 2013. Onset of deglacial warming in West Antarctica driven by
800 local orbital forcing. *Nature*, **500**(7463): 440-444.

801 Whillans, I.M., Jezek, K.C., Drew, A.R. and Gundestrup, N.: Ice flow leading to the deep core
802 hole at dye-3, greenland. *Annals of Glaciology*, **5**: 185-190, 1984

803 Winski, D. A., Fudge, T. J., Ferris, D. G., Osterberg, E. C., Fegyveresi, J. M., Cole-Dai, J.,
804 Thundercloud, Z., Cox, T. S., Kreutz, K. J., Ortman, N., Buizert, C., Epifanio, J., Brook, E.
805 J., Beaudette, R., Severinghaus, J., Sowers, T., Steig, E. J., Kahle, E. C., Jones, T. R., Morris,
806 V., Aydin, M., Nicewonger, M. R., Casey, K. A., Alley, R. B., Waddington, E. D., Iverson,
807 N. A., Dunbar, N. W., Bay, R. C., Souney, J. M., Sigl, M., and McConnell, J. R.: The SP19
808 chronology for the South Pole Ice Core – Part 1: volcanic matching and annual layer
809 counting, *Clim. Past*, 15, 1793–1808, <https://doi.org/10.5194/cp-15-1793-2019>, 2019.

810